

Potassium hydroxide polishing of nanoscale deep reactive-ion etched ultrahigh aspect ratio gratings

Alexander Bruccoleri,^{a)} Dong Guan, Pran Mukherjee, Ralf K. Heilmann, and Mark L. Schattenburg

Space Nanotechnology Laboratory, MIT Kavli Institute for Astrophysics and Space Research, Massachusetts Institute of Technology, Cambridge, Massachusetts 02139

Stephen Vargo

SPTS Technologies, Inc., 1150 Ringwood Ct., San Jose, California 95131

(Received 21 June 2013; accepted 26 August 2013; published 12 September 2013)

A fabrication process has been developed to chemically polish the sidewalls of 200 nm-pitch gratings via potassium hydroxide (KOH) etching following the Bosch deep reactive-ion etching (DRIE) process. Previous KOH polishing experiments focused on micron scale features. This work is the first reported combined DRIE-KOH etching process on the nanoscale for ultrahigh aspect ratio structures with feature sizes 30 times smaller than previously published work. The primary application of the gratings is x-ray spectroscopy and requires polished sidewalls for efficient x-ray reflection. Polishing is also critical for increasing the open area by narrowing the grating bars, which increases the throughput of x-rays. The increased open area is also valuable for other applications such as ultraviolet filtration, neutron spectroscopy and biofiltration. Advanced Bosch processes leave approximately 4 nm, root mean square (RMS), of roughness on the sidewalls. This roughness needs to be reduced to below 1 nm to efficiently reflect soft x-rays with wavelengths between 1 and 5 nm. Furthermore, high aspect ratio DRIE can result in bar width variations of approximately a factor of two from the top to the middle of the channel, commonly referred to as bowing. The polishing procedure presented here removes the roughness to below the resolution of the scanning electron microscope, and was measured via an atomic force microscope to be less than 1 nm RMS. The bowing has also been reduced by at least a factor of 3. The polishing process takes advantage of the anisotropy of KOH silicon etching. Specifically, the {111} silicon planes etch approximately 100 times slower than other crystal planes. This anisotropy allows the grating bars to be etched in 50% by weight KOH at room temperature for up to 60 min. Long etches have several key requirements, including 0.2 degree alignment of the grating with respect to the {111} planes, mask roughness below 40 nm and minimal defects in the silicon. If these requirements are not met, the grating will quickly be destroyed by the etch, which etches the non-{111} planes in excess of 1 μm per hour. The fabrication steps of this work are described in detail including a novel technique to align the 200 nm-pitch interference lithography image grating to the {111} planes of a $\langle 110 \rangle$ silicon wafer. © 2013 American Vacuum Society. [<http://dx.doi.org/10.1116/1.4820901>]

I. INTRODUCTION

This paper presents a process for chemically polishing the sidewalls of nanoscale ultrahigh aspect ratio gratings, as described in detail by Bruccoleri.¹ Specifically, the gratings are 200 nm-pitch, and etched via the Bosch deep reactive-ion etch (DRIE) process to a depth of 4 μm , with an RMS roughness of 4 nm as measured with an atomic force microscope (AFM). Past work led to large area (31 mm on a side) freestanding gratings in a monolithic structure from a silicon-on-insulator wafer with a 5 μm -pitch level 1 cross support grating in the device layer with the 200 nm-pitch grating, and an array of 1 mm-wide hexagons providing another level of support in the handle layer.² See Fig. 1 for SEM imagery of the freestanding grating with rough sidewalls. The primary application of the polishing process is to reduce the sidewall roughness to 1 nm RMS for the critical-angle transmission (CAT) grating, a component of future high-efficiency space-

based x-ray spectrometers. The specific energy band of interest is between 0.2 and 1 keV, also referred to as soft x-rays, which covers emission lines of iron, carbon, neon, nitrogen, and oxygen.³ Other applications include phase contrast imaging,⁴ ultraviolet filtration,⁵ and neutral mass spectroscopy.⁶

The CAT grating is a hybrid design between a blazed reflection grating and a transmission grating. The angles of the diffraction orders can be derived geometrically, obtaining

$$m\lambda = P(\sin(\theta_i) + \sin(\beta_m)), \quad (1)$$

where m is the diffraction order, λ is the wavelength, P is the grating period, θ_i is the grazing angle of incidence and β_m is the angle of the outgoing diffraction orders relative to the grating bar sidewalls (see Fig. 2). The key idea is to transmit the x-rays through the grating at a shallow angle where they reflect such that the angles of diffraction orders coincide with the specular reflection angle. This effect is known as blazing, and it can significantly increase efficiency since the

^{a)}Electronic mail: alexbruc@alum.mit.edu

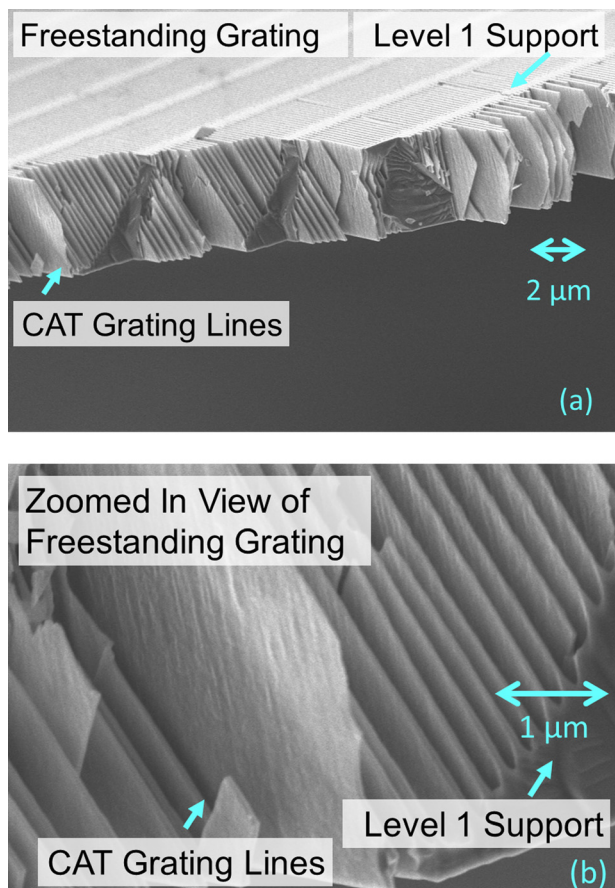


FIG. 1. (Color online) Slanted SEM images of torn freestanding CAT grating film. The roughness in the CAT grating sidewalls can be observed. (a) Freestanding grating. (b) Zoomed in on rough sidewall.

majority of the light is directed into a small number of non-zero diffraction orders. The transmission gratings onboard the Chandra x-ray telescope, made of gold on a membrane, represent the state-of-the-art in space-based phase-shifting x-ray transmission gratings and absorbed soft x-rays reducing their efficiency.^{7,8} The CAT grating reflects the majority of the x-rays significantly reducing absorption losses enabling a boost in efficiency by a factor of five in the soft x-ray band over the Chandra gratings.⁹

A key detail of the CAT grating to be efficient is the x-rays must reflect at or below the critical angle for total external reflection. Soft x-rays usually have an index of refraction, n , slightly less than one in solid materials

$$n = 1 - \delta + i\beta, \quad (2)$$

where δ and β are both small and functions of the material and x-ray wavelength. For example, δ of silicon is approximately 4×10^{-4} for λ of 1 nm.¹⁰ Since the real part of the index of refraction is less than one, an incident x-ray can have a grazing angle of incidence θ that results in total external reflection. Figure 3 shows a conceptual drawing of x-ray refraction. This effect is equivalent to total internal reflection for optical light at the interface between a solid material such as glass and vacuum. The largest angle for total external reflection is referred to as the critical angle for total

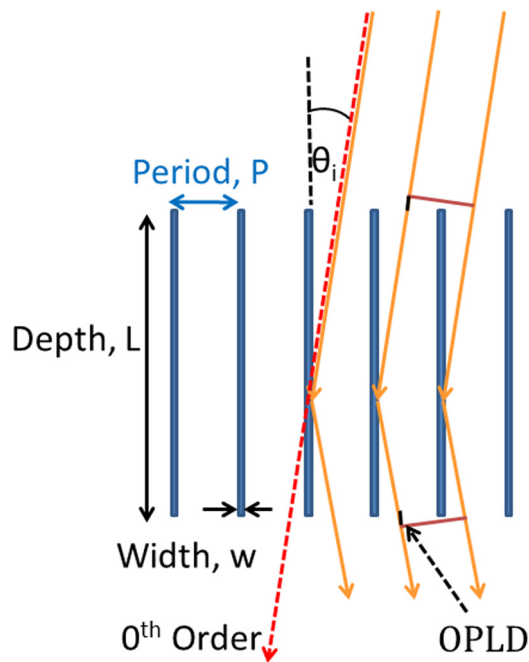


FIG. 2. (Color online) Conceptual geometric drawing of CAT grating cross section (not to scale).

external reflection θ_c , ($\theta_c \approx \sqrt{2\delta}$). For silicon this leads to $\theta_c \approx 1.6^\circ$ for λ of 1 nm, which is a very shallow angle, and leads to the required ultrahigh aspect ratio for CAT grating bars.

In addition to requiring shallow graze angles, the surfaces also have to be smooth for efficient x-ray reflectivity. The efficiency of reflection is an exponential function of roughness

$$R(q) = R_o e^{-q^2 \sigma^2}, \quad (3)$$

where R is the reflectivity, R_o is the reflectivity from a perfectly smooth surface, q is the momentum transfer of the reflection, and σ is the roughness. The momentum transfer from a specular x-ray reflection is given by

$$q = \frac{4\pi}{\lambda} n \sin \theta, \quad (4)$$

where n is the index of refraction of the material for the incident x-ray, and θ is the angle of grazing incidence. For an

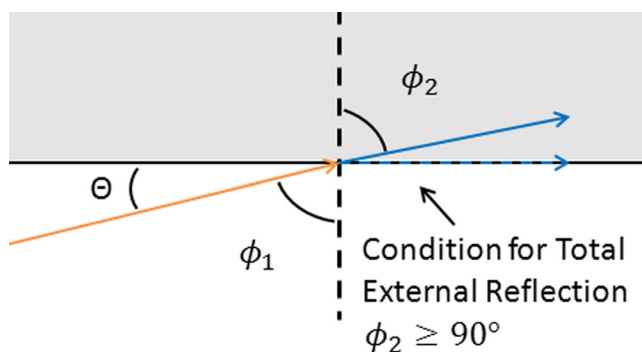


FIG. 3. (Color online) Conceptual drawing of x-ray refraction and condition for total external reflection (not to scale).

x-ray with λ of 1 nm, and grazing incidence angle of 1.6° , the roughness needs to be on the order of 1 nm for a 90% efficient reflection. This requirement of surface roughness is the primary motivation for the polishing process. Furthermore, the polishing process narrows the grating bars, which increases the open-area fraction of a freestanding grating.

KOH polishing is a promising solution in previously published work for smoothing the sidewalls of features created via DRIE. Defforge *et al.* performed a series of experiments with both KOH and tetramethylammonium hydroxide at concentrations of 2 and 5% mixed with isopropyl alcohol (IPA) at 10 and 20% by weight.¹¹ The low concentration etches were done at 10°C and higher concentration at 22°C . All etches were done for 16 h. They reported the best result with 5% KOH and 20% IPA, which reduced the roughness from 178 to 2.8 nm RMS and 707 to 14.8 nm peak-to-peak. These were holes approximately $12\ \mu\text{m}$ wide and the faces etched were both $\{110\}$ and $\{100\}$. Jeong *et al.* demonstrated a process for the narrowest ($3.7\ \mu\text{m}$) reported features to be KOH polished after DRIE.^{12,13} This process was developed to reduce the roughness of oblique comb electrodes from 200 to 20 nm RMS. The process also used the $\{111\}$ planes on a $\langle 110 \rangle$ wafer to reduce the etch rate on the polished surface. Their etch solution was 45% KOH by weight at 75°C for 10 m.

The present work is the first published combined DRIE–KOH etching process on the nanoscale for ultrahigh aspect ratio structures. The CAT grating bars started out 100 nm wide and were reduced to less than 70 nm while all detectable roughness was removed as judged by SEM inspection. These features are over 30 times smaller than features published to date. Furthermore, high aspect ratio DRIE can result in bar-width variations of approximately a factor of two from the top to the middle of the channel, commonly referred to as bowing. Bowing has also been reduced by at least a factor of 3 via the polishing process.

II. FABRICATION METHODOLOGY

The presented polishing process is very delicate and many experiments were done to debug the process. The polishing process takes advantage of the anisotropy of KOH silicon etching, specifically the significant reduction of the $\{111\}$ silicon planes' etch rate. This anisotropy allows the grating bars to be etched in 50% by weight KOH at room temperature for up to 60 min. Long etches have several key requirements, including ± 0.2 degree alignment of the grating with respect to the $\{111\}$ planes, mask roughness below 40 nm and minimal defects in the silicon. If these requirements are not met, the grating will quickly be destroyed by the etch, which etches the non- $\{111\}$ planes in excess of $1\ \mu\text{m}/\text{h}$.¹⁴ The wafers were $\langle 110 \rangle$ silicon. Both Czochralski (CZ) and float-zone (FZ) silicon were used in the experiments with no consistent difference in the results although limited experiments were done with FZ silicon.

A. Alignment requirements

Ideally each grating bar should be bound by two $\{111\}$ planes, the top mask, bottom SiO_2 and the level 1 supports,

which also form $\{111\}$ planes. Assuming the final bar-width target is 40 nm, and given a level 1 cross support pitch of $5\ \mu\text{m}$, the alignment needs to be on the order of 0.2° in the top plane of the wafer. See Fig. 4(a) for a drawing depicting this alignment. The sample also needs to have the deep etch

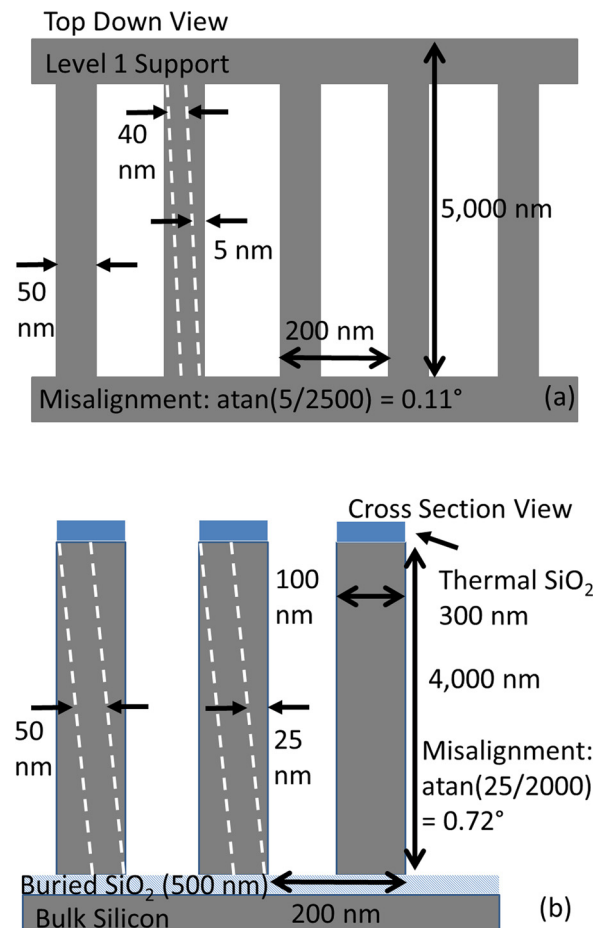


Fig. 4. (Color online) Drawing and SEM imagery depicting the two axis of grating alignment. (a) Drawing of top down alignment. (b) Drawing of vertical alignment. (c) SEM image of vertical alignment.

go vertically down within a tolerance of 0.7° . The latter is controlled by the wafer manufacturer, and wafers can be purchased with an alignment of the $\langle 110 \rangle$ vector to vertical within 0.25° . See Figs. 4(b) and 4(c) for drawings and SEM imagery depicting this alignment. The former requirement is partially driven by the bowing of the deep etch. The minimum bar-width of the deep etch was approximately 50 nm, which constricted the alignment since little material remained for a 40 nm-wide bar to be misaligned.

B. Locating $\{111\}$ planes

The first step in the alignment process is to locate the $\{111\}$ planes. Wafers sliced to $\langle 110 \rangle$ orientation have a major flat on the $\langle 111 \rangle$ orientation. This flat is not precise as it is often curved such that repeatable alignment to within a large angle of 1° is not often possible. To address this a fan-shaped pattern referred to as a wagon wheel is patterned near the edge of the wafer with spokes at angular increments of 0.05° , and approximately $6\ \mu\text{m}$ channel-widths. This wagon wheel is a scaled down version of the same wagon wheel used in Ahn's process.¹⁵ The wagon wheel spans $\pm 3^\circ$ and is aligned to the major flat within 1° via an optical microscope during contact lithography. The wagon wheel pattern is then etched into the thermal SiO_2 or low-pressure chemical vapor deposition (LPCVD) Si_3N_4 mask depending on the experiment. The sample is then placed in 50% KOH such that only the wagon wheel is submerged. It is left in room temperature KOH for approximately 30 h in order to etch away wagon-wheel spokes that are misaligned by more than 1° . (Etches between 24 and 36 h would all yield reasonable results, which makes this process reliable with a large window for success.) The remaining spokes showed clear line-width variations from lateral etching, and the widest spoke was very easy to observe in an optical microscope. The orientation of the best spoke corresponds to the direction to which the CAT grating line should be aligned. Figure 5 shows optical microscope images of a KOH etched wagon wheel. In this example, the $\{111\}$ plane is at $+0.05^\circ$, which means the optical lithography was nearly perfectly aligned to the $\{111\}$ plane. The error in this technique is approximately 0.10° and is subject to human error.

This wagon wheel technique is an improvement to a similar technique implemented by Ahn.¹⁵ The former process used a wagon wheel roughly four times larger that was etched in 25% KOH at 80°C for 30 min and the bars were undercut from lateral etching. This effect was observable from top-down observations in an SEM. An estimate of the undercut was made along many spokes, and a graph was generated with undercut versus spoke angle. A curve fit was made and the minimum undercut was located. The newer process is significantly more efficient as the best wagon wheel spoke can be observed optically and found within a minute of observation. The old method would take roughly an hour in an SEM to inspect enough spokes to make a plot. Furthermore, another short coming of the old technique was difficulty in determining the exact undercut due to chipping away of micron-scale chunks in the mask.

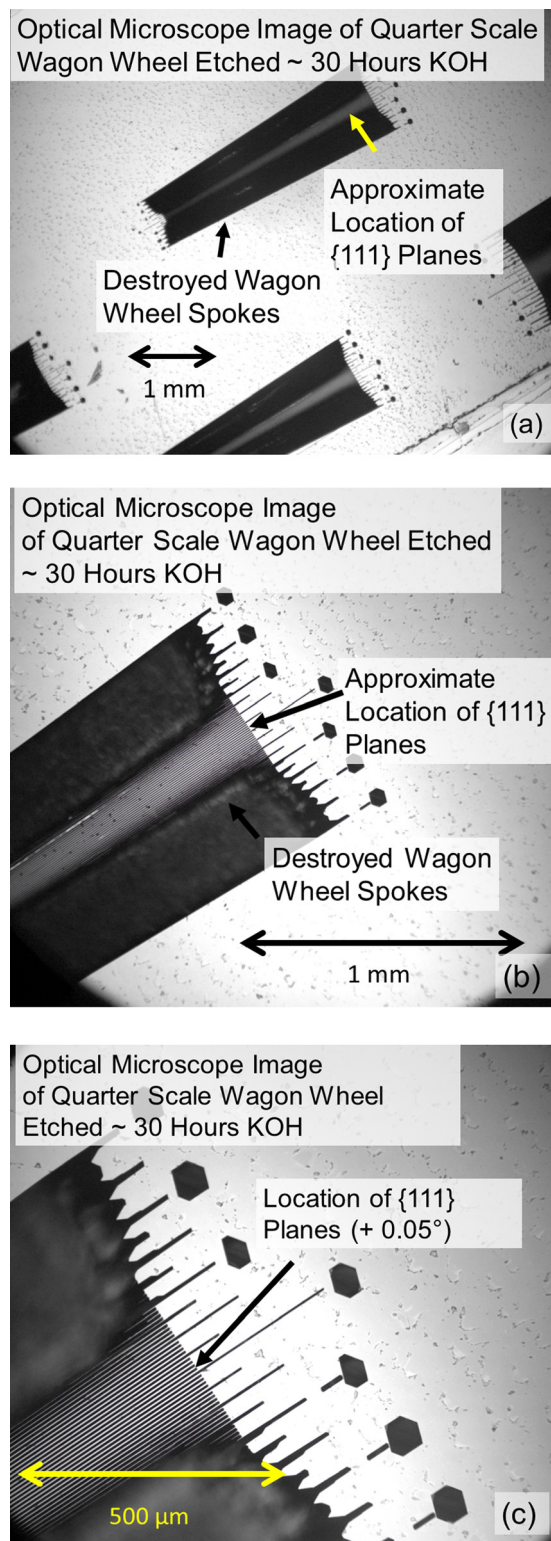


Fig. 5. (Color online) Optical microscope imagery of KOH etched wagon wheels. The images show progressive increases in magnification and the $\{111\}$ plane can be identified in image (c) at $+0.05^\circ$. (a) Zoomed out wagon wheel. (b) Zoomed in wagon wheel. (c) Zoomed in wagon wheel with $\{111\}$ plane identified.

C. Aligning grating lines to $\{111\}$ planes

The 200 nm-pitch CAT grating lines are aligned to the $\{111\}$ planes using a novel technique via a Mach-Zehnder

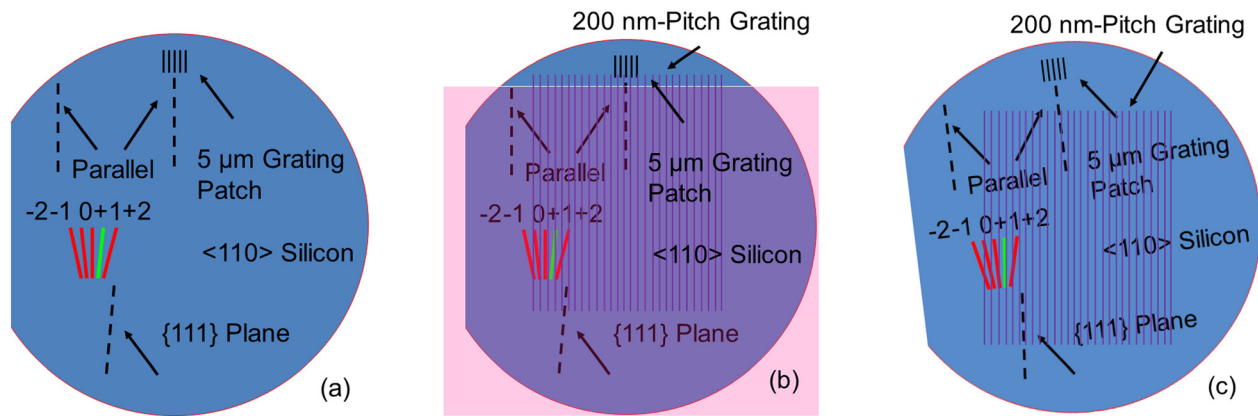


FIG. 6. (Color online) Drawings depicting various stages of the alignment process. (a) Depicts the wafer after the wagon has been pre etched via KOH. (b) Depicts CAT grating parallel to the $5\ \mu\text{m}$ grating patch. (c) Depict the CAT grating lines exposed parallel to the $\{111\}$ planes.

interference lithography table.¹⁶ See Fig. 6 for a sequence of drawings for the alignment process. A $5\ \mu\text{m}$ -pitch grating patch, 2 mm on a side, was patterned on the upper region of the wafer. This grating is patterned via contact lithography via the same mask as the wagon wheel and is parallel to the 0° wagon wheel spoke. This grating patch is etched into the silicon to a depth of approximately $1\ \mu\text{m}$. The concept is to generate an array of diffraction orders via this grating patch, from each arm of the interferometer. The angle of the diffraction order array will vary as the grating is rotated. When the array of diffraction orders from each arm overlap the two incident arms are at the same angle relative to the grating, and the standing waves (200 nm-pitch image grating used to pattern the CAT grating lines) are parallel to the grating patch. A camera is used to image the diffraction orders in real time. The majority of the wafer to be patterned is covered via a 150 mm wafer coated with anti reflective coating during the alignment step to prevent premature exposure, which is depicted by the pink square in Fig. 6(b). Once the image grating lines are parallel to the grating patch, the wafer can be rotated on a vernier chuck by the amount determined in the KOH pre etch. The chuck has a precision of 0.017° ; however, user error caused this to be closer to 0.10° . With the error in the wagon wheel technique the total error is 0.14° and 0.20° is used as a conservative number. This requires the minimum bar-width to be approximately 58 nm as described by the requirements in Sec. II A.

D. Improved deep etch for KOH polishing $4\ \mu\text{m}$ -deep, 200 nm-pitch gratings

An improved DRIE process was developed in order to address the bowing of the process developed by Mukherjee *et al.*¹⁷ This new process significantly reduced the bowing of the deep etch and the minimum bar-width was increased to 100 nm. The new process increased the passivation step duration by 50% and decreased the coil power by 25%. The etch step is made more potent by increasing the coil power by 36% and decreasing the ratio of C_4F_8 to SF_6 . The selectivity of the etch decreased, which was the only drawback of the process, and almost no mask remained at a depth of $4\ \mu\text{m}$. The process parameters of the former and improved

etch are given in Table I, and see Figs. 7 and 8 for SEM imagery of both etches. The masks in Fig. 7 is approximately 30 nm of LPCVD Si_xN_y with 30 nm chrome and the mask in Fig. 8 is 300 nm of thermal SiO_2 . No difference was observed in the bowing phenomenon with these two masking materials.

E. KOH polishing

After the DRIE step, the samples undergo a four-step clean prior to polishing: piranha to remove the majority of the organic contamination, CR-7 to remove the chrome (if chrome masks are used), $\sim 100\ \text{ml}$ 3M Novec 7200 [$\text{C}_4\text{F}_9\text{OC}_2\text{H}_5$ (Ref. 18)] on a hot plate set for 200°C for 10 min to remove the Bosch process polymer and 50:1 DI water:HF for 60 s to remove native SiO_2 . Following the clean step, the samples are etched in 50% KOH by weight at room temperature and rinsed in DI water. Finally the samples are either dried via a nitrogen gun for inspection or critical-point dried if further processing is planned to avoid damage from liquid–air surface tension forces.

III. KOH POLISHING RESULTS

A. KOH polishing $3\ \mu\text{m}$ -deep, 200 nm-pitch gratings

The initial successful polishing results at 200 nm-pitch had been deep etched to a depth of approximately $2.5\ \mu\text{m}$. These tests were done with the older DRIE process and bowing prevented deeper etches. The mask was 20 nm chrome on 30 nm LPCVD Si_xN_y , with a duty cycle in excess of 75%.

TABLE I. Improved nanoscale DRIE parameters (values in parentheses are from the older process).

Device parameter	Deposition cycle	Etch cycle
SF_6 flow rate (SCCM)	(0)0	(200) 175
C_4F_8 flow rate (SCCM)	(150) 150	(80) 50–25
Coil power (W)	(2000) 1500	(1100) 1500
Platen power (W)	(0)0	(30–60) 50–65
Cycle time (s)	(1) 1.5	(1.5) 1.5
Base pressure (mTorr)	(7.5) 10	(7.5) 10
Chuck temperature ($^\circ\text{C}$)	(–15) –15	(–15) –15

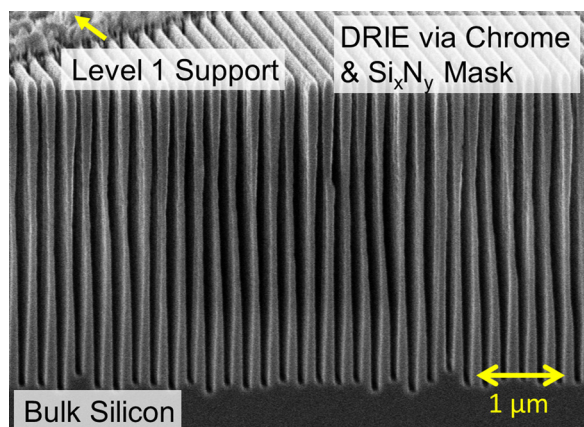


Fig. 7. (Color online) SEM image of 200 nm-pitch grating etched via the old process. Observe the narrow waist from bowing.

The deep etch was similar to the old process in Table I except the platen power was ramped from 30 to 57 W and the time was 10 min. The narrow channels resulted in a shallow etch and there was plenty of bar-width at the minimum point for subsequent KOH polishing. See Fig. 9 for a time series of an early polishing experiment. The etch times are 15, 30, and 60 min. The reduction in bowing with time can be observed. See Fig. 10 for SEM imagery before and after a

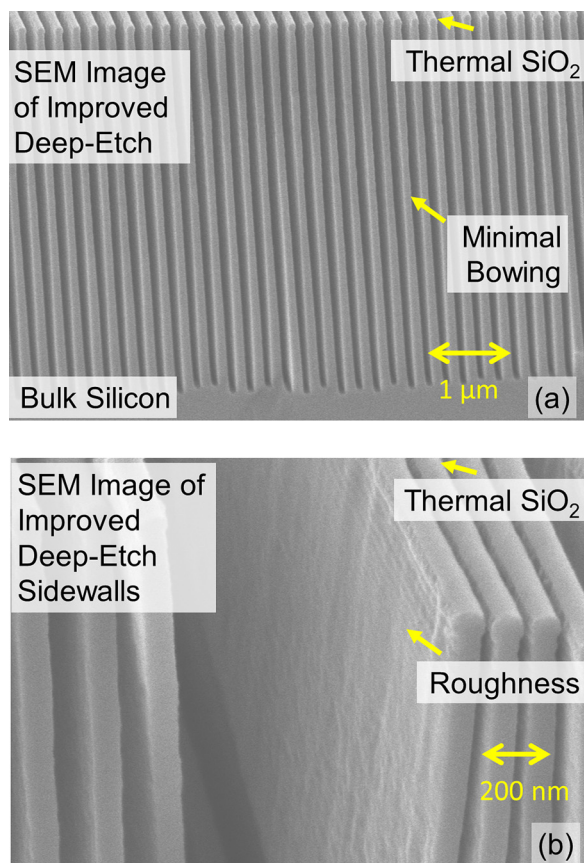


Fig. 8. (Color online) Cross section SEM imagery of improved deep-etch process. This sample was etched for 9 min 30 s and was not used for later polishing experiments. A sidewall was observed to show roughness. (a) Zoomed out; (b) zoomed in sidewall.

20 min duration KOH polish. This experiment used 0.02% surfactant, sodium dihexyl sulfosuccinate to reduce the surface tension in the solution and reduce the effect of H_2 bubbles from sequestering and resulting in uneven etching.¹⁵ These results show a near perfect reduction of bowing and the roughness is below the resolution of the SEM.

B. Improved KOH polishing 4 μm -deep, 200 nm-pitch gratings

The new deep-etch process enabled a much longer polishing step, with grating depths etched in excess of 4 μm , due to the increased minimum bar-width and reduction in roughness. The longest polishing step was for 43 min with 50% KOH and surfactant. The grating was cleaned with the same process except no CR-7 was required since the mask was thermal SiO_2 . The KOH solution was also the same. The grating roughness was eliminated as judged by SEM observation. The line-width was reduced to less than 40 nm at the top of the grating bar and less than 70 nm at a depth of 4 μm . The maximum depth of the polished grating bar was approximately 5 μm , since the KOH etched vertically downward as well as polished the sidewalls. See Fig. 11 for SEM imagery of the 43 min duration KOH polish.

C. AFM data for polished 4 μm -deep, 200 nm-pitch gratings

In order to quantify the sidewall roughness, an AFM was used to scan the sidewall. A polishing experiment was done on a 200 nm-pitch grating that was etched on the 4 μm device layer of an SOI wafer. The deep etch was done for 7 min with the improved process in Table I, and the sample was polished in 50% KOH and surfactant for 30 min, and cleaved parallel to the grating lines. The polishing step was shorter to be conservative since the mask had a duty cycle below 40%. (The results from the 43 min polish would presumably be smoother due to the longer polishing step.) The cleaved cross section was mounted face up and scanned over different regions of the grating sidewall. The cleave damaged the sidewalls and complete scans were not possible. Furthermore, several grating bars are cleaved between level 1 supports as seen in Fig. 12, which also prevented large areas from being scanned. Regions spanning 1 μm on a side were scanned and the RMS roughness was measured to be approximately 4 nm prior to polishing and between 0.7 and 1.5 nm after polishing, which is in the range necessary to reflect soft x-rays. See Fig. 12 for example AFM data of the grating sidewalls. These results are preliminary; however, they quantify the sidewall roughness and corroborate the SEM imagery that the smoothness is approximately 1 nm.

IV. ANALYSIS OF FAILED POLISHING ATTEMPTS

It was known a priori that the masks would need to be aligned to the {111} planes, and the line-edge roughness needed to be small enough to allow for enough silicon material to be polished between the peaks and valleys of the roughness. During the development process, many other issues were discovered.

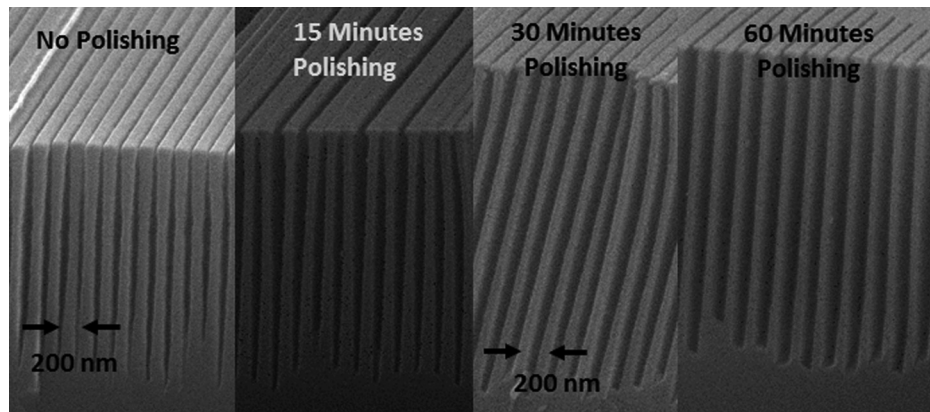


FIG. 9. Cross section SEM imagery of a time series experiment for KOH polishing. These experiments utilized FZ silicon and ultrasonic agitation.

Most notably, ultrasonic agitation was discovered to damage and ultimately destroy the grating bars during polishing. See Fig. 13 for an SEM image of a grating destroyed from 5 min of KOH polishing with ultrasonic agitation. A former process developed by Ahn to etch small open-area fraction CAT gratings purely with KOH etching utilized ultrasonic agitation.¹⁵ This failure mode was particularly challenging to discover since the results were not consistent. The strength of the ultrasound can vary depending on where the sample is placed in the beaker, the beaker type and how it is physically mounted.

As mentioned previously, the bowing also led to destructive polishing results. Line-edge roughness in the mask coupled with a narrow waist left little room to enclose enough silicon material between two {111} planes and the centers of the grating bars would be etched and eventually destroyed during polishing. See Fig. 14 for an SEM image of the grating in Fig. 7 polished for 30 min and destroyed in 50% KOH. The line-edge roughness in the mask is likely due to a combination of the initial patterning of the photoresist and pattern transfer steps into the thermal SiO₂.¹⁷ Ahn *et al.* proposed mask roughness with LPCVD Si_xN_y as the

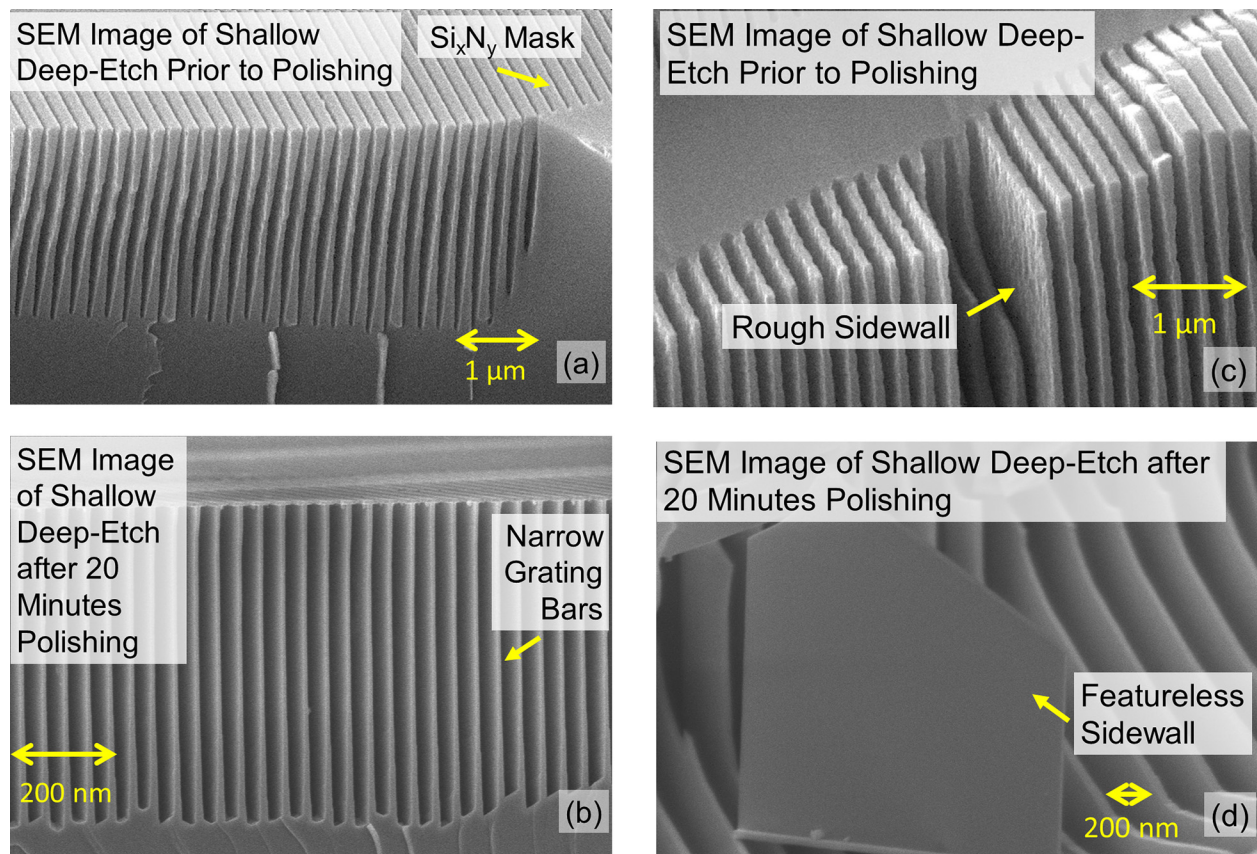


FIG. 10. (Color online) Cross section SEM imagery of 200 nm-pitch, 2.5 μm deep grating polishing experiment with CZ silicon. (a) No polishing; (b) cross section after polishing; (c) no polishing; (d) zoomed in sidewall after polishing.

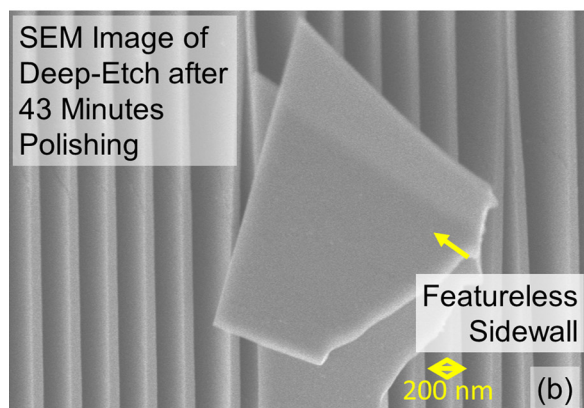
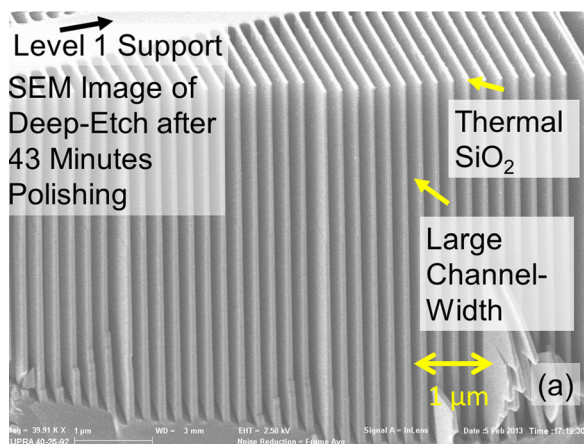


Fig. 11. (Color online) Cross section SEM imagery of polished 200 nm-pitch, 4 μm deep gratings. A sidewall was observed to show improved smoothness. (a) Zoomed out; (b) zoomed in.

material to be a possible cause of rapid undercut with a KOH process to fabricate CAT gratings.¹⁴ This suggests thermal SiO₂ is not the sole cause of the line-edge roughness. The line-edge roughness adds to the roughness caused by the Bosch process and it is likely that reducing the initial mask line-edge roughness via improved lithography and pattern transfer could improve the final sidewall roughness after KOH polishing.

Additionally, several other factors were observed and suspected to prevent successful polishing. Insufficient cleaning of the gratings likely due to the Bosch polymer prevented even polishing during initial tests. HF cleaning to remove native SiO₂ could be too aggressive and thin down thermal SiO₂, or undercut LPCVD Si_xN_y masks which have been reported to have nanometer-scale films of SiO₂ between the silicon and Si_xN_y during deposition.¹⁹ Destructive polishing results were observed when removing the samples and allowing them to contact the air when transferring them between beakers. The likely cause is surface tension forces which are believed to bend the gratings, possibly cracking them and damaging the crystal lattice.

V. CONCLUSION

Several experiments were conducted to demonstrate that 200 nm-pitch silicon gratings, deep etched via the Bosch

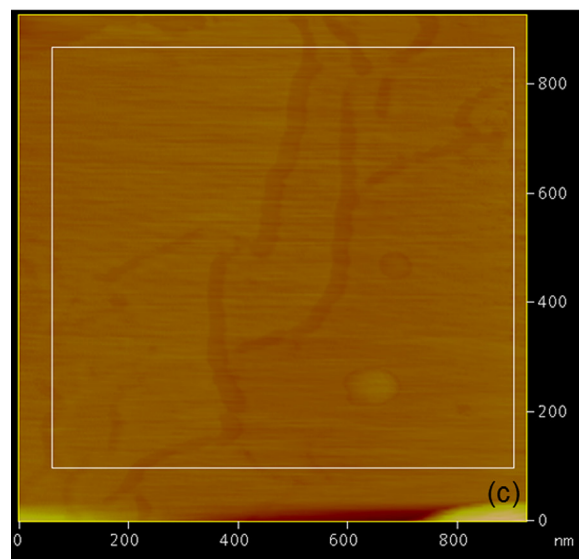
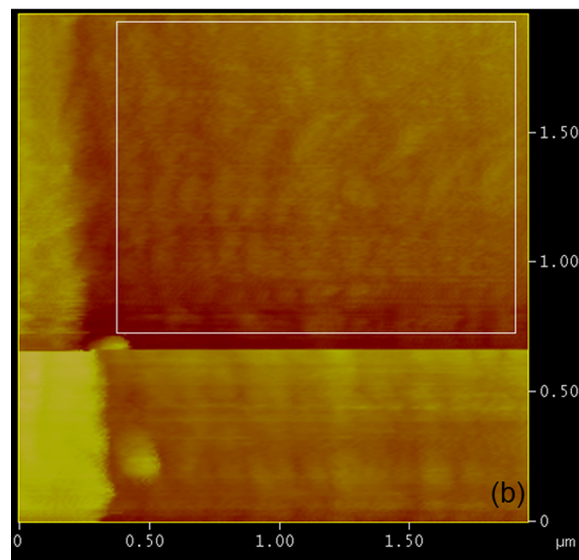
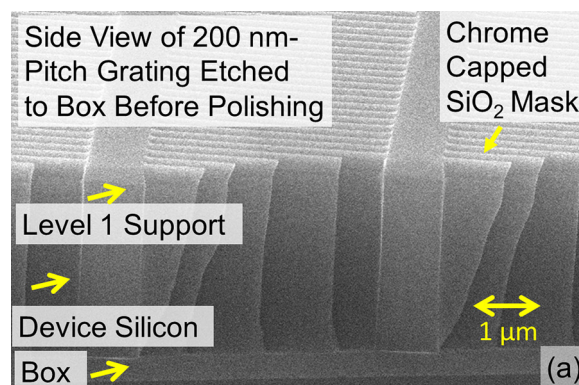


Fig. 12. (Color online) SEM image and AFM data of both unpolished and polished sidewalls. (a) Side view SEM image no polishing. (b) AFM image no polishing, RMS roughness measured at 4.3. (c) AFM image 30 min polishing, RMS roughness measured at 1.1 nm.

process to 4 μm, could be KOH polished. The polishing reduced the sidewall roughness from approximately 4 to 1 nm RMS and reduced the size of the grating bars from 100 to less than 70 nm. This line-width reduction demonstrated

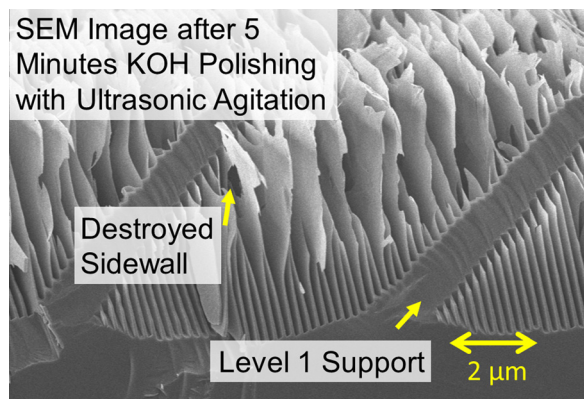


FIG. 13. (Color online) Cross section SEM imagery of 200-nm-pitch, 4 μm deep grating polishing experiment after 5 min KOH polishing with ultrasonic agitation.

that KOH polishing is a feasible method to increase the open-area fraction of the CAT grating. These results are preliminary and a more refined deep etch and longer polishes will further increase the open-area fraction. These experiments led to innovations in lithography, deep etching, and a better understanding of KOH etching nanoscale features. A novel alignment technique was developed to use a Mach-Zehnder interferometer in combination with a pre-etched wagon wheel to align the 200-nm-pitch grating lines within 0.2° to the {111} silicon planes. An improved deep etch was developed to enable 200-nm-pitch lines to be etched to a depth of 4 μm with a minimum bar-thickness of 100 nm. The grating bars are fragile, and ultrasonic agitation was discov-

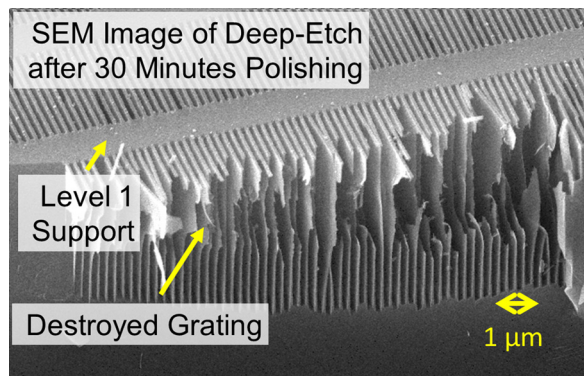


FIG. 14. (Color online) Cross section SEM imagery of 200-nm-pitch, 3.5 μm deep grating polishing experiment after 30 min KOH.

ered to cause damage and prevent reliable deep etches. Furthermore, the samples needed to be processed carefully to avoid mechanical damage. All of these factors were important to enable a sufficient polishing process.

ACKNOWLEDGMENTS

This work was funded by NASA Grant Nos. NNX08AI62G, NNX11AF30G, and NNX12AF21G, the MIT Kavli Institute, and the Department of Defense National Defense Science and Engineering Graduate (NDSEG) fellowship program. Specific thanks to James Daley of the MIT Nanostructures Lab, Vicky Diadiuk, Dennis Ward, Dave Terry, and Paul Tierney of the Microsystems Technology Laboratories, and Brian VanDerElzen of the University of Michigan Lurie Nanofabrication Facility.

- ¹A. Bruccoleri, Ph.D. dissertation, Massachusetts Institute of Technology (2013).
- ²A. Bruccoleri, P. Mukherjee, R. K. Heilmann, J. Yam, M. L. Schattenburg, and F. DiPiazza, *J. Vac. Sci. Technol. B* **30**, 06FF03 (2012).
- ³R. K. Heilmann *et al.*, *Proc. SPIE* **7732**, 77321J (2010).
- ⁴C. David, J. Bruder, T. Rohbeck, C. Grunzweig, C. Kottler, A. Diaz, O. Bunk, and F. Pfeiffer, *Microelectron. Eng.* **84**, 1172 (2007).
- ⁵J. T. M. van Beek, R. C. Fleming, P. S. Hindle, J. D. Prentiss, M. L. Schattenburg, and S. Ritzau, *J. Vac. Sci. Technol. B* **16**, 3911 (1998).
- ⁶D. W. Keith, M. L. Schattenburg, H. I. Smith, and D. E. Pritchard, *Phys. Rev. Lett.* **61**, 1580 (1988).
- ⁷C. R. Canizares, M. L. Schattenburg, and H. I. Smith, *Proc. SPIE* **597**, 253 (1986).
- ⁸F. Paerels, *Space Sci. Rev.* **157**, 15 (2010).
- ⁹R. K. Heilmann, M. Ahn, and M. L. Schattenburg, *Proc. SPIE* **7011**, 701106 (2008).
- ¹⁰E. Spiller, *Soft X-Ray Optics* (SPIE Optical Engineering Press, Bellingham, WA, 1994).
- ¹¹T. Defforge, X. Song, G. Gautier, T. Tillocher, R. Dussart, S. Kouassi, and F. Tran-Van, *Sens. Actuators A* **170**, 114 (2011).
- ¹²D.-H. Jeong, S.-S. Yun, M.-L. Lee, G. Hwang, C.-A. Choi, and J.-H. Lee, in *IEEE 22nd International Conference on Micro Electro Mechanical Systems*, 2009, MEMS 2009, pp. 797–800.
- ¹³D.-H. Jeong, S.-S. Yun, B.-G. Lee, M.-L. Lee, C.-A. Choi, and J.-H. Lee, *J. Microelectromech. Syst.* **20**, 1269 (2011).
- ¹⁴M. Ahn, R. K. Heilmann, and M. L. Schattenburg, *J. Vac. Sci. Technol. B* **26**, 2179 (2008).
- ¹⁵M. Ahn, Ph.D. dissertation, Massachusetts Institute of Technology (2009).
- ¹⁶M. L. Schattenburg, E. H. Anderson, and H. I. Smith, *Phys. Scr.* **41**, 13 (1990).
- ¹⁷P. Mukherjee, A. Bruccoleri, R. K. Heilmann, M. L. Schattenburg, A. Kaplan, and L. Guo, *J. Vac. Sci. Technol. B* **28**, C6P70 (2010).
- ¹⁸P. G. Clark, E. D. Olson, and H. Kofuse, in *International Conference on Soldering and Reliability*, Toronto, Ontario, Canada (2009).
- ¹⁹F. H. P. M. Habraken, A. E. T. Kuiper, A. V. Oostrom, Y. Tamminga, and J. B. Theeten, *J. Appl. Phys.* **53**, 404 (1982).